Acta Crystallographica Section B
Structural Science
ISSN 0108-7681

Bond catastrophes in rhodium complexes: experimental charge-density studies of $[Rh(C_7H_8)(P^tBu_3)Cl]$ and $[Rh(C_7H_8)(PCy_3)Cl]$

Hazel A. Sparkes,[a]* Adrian B. Chaplin,[b] Andrew S. Weller[b] and Judith A. K. Howard[a]

[a]Durham University Department of Chemistry, University Science Laboratories, South Road, Durham DH1 3LE, England, and [b]University of Oxford, Inorganic Chemistry, South Parks Road, Oxford OX1 3QR, England

Correspondence e-mail: h.a.sparkes@durham.ac.uk

Received 27 April 2010
Accepted 5 August 2010

Rhodium complexes have potential uses in both catalysis and promoting the cleavage of C—C bonds. In order to further our understanding of these species and their potential applications, it is vital to obtain insight into the bonding within the species, particularly the Rh—C interactions, and to this end experimental charge-density studies have been undertaken on the title complexes. High-resolution single-crystal datasets to $\sin\theta/\lambda = 1.06$ Å^{-1} were obtained at 100 K and analysed using Bader's 'Atoms in Molecules' (AIM) approach. The results of the studies have provided unique insights into the bonding involving rhodium and highlight the importance of undertaking such investigations for transition metal compounds.

1. Introduction

Transition metal complexes have many important catalytic applications as well as promoting the cleavage of C—C bonds. The latter application allows strong C—C bonds to be broken and subsequently functionalized, which is of particular use in organic chemistry (Jun, 2004). Rybtchinski & Milstein (1999) suggested using strained species such as cyclopropanes as one method of achieving metal-promoted C—C activation. In such approaches, the reduction in the strain of the system accompanying the cleavage of the C—C bonds is thought to provide the driving force to overcome the thermodynamic and kinetic barriers to the process. Our interest in rhodium complexes arose from their potential C—C bond activation properties, such processes pass through putative intermediates with Rh···(C—C) sigma interactions. Although it is tricky to isolate such intermediates, we have used X-ray diffraction to structurally characterize several examples of these species including $[Rh(PR_3)(\text{binor-S})][BAr^f_4]$ (Brayshaw *et al.*, 2007). In order to gain further understanding of the species it is crucial to examine the nature of the bonding involving rhodium.

Experimental charge-density studies offer the potential to gain vital insights into the nature of the bonding and interactions in the compound under study. Such studies are challenging, requiring carefully collected high-resolution X-ray diffraction data from good quality single crystals followed by detailed analysis of the refinement results. Bader's quantum theory of Atoms in Molecules (AIM; Bader, 1990) is an invaluable tool in the analysis of the chemical interactions between atoms, classifying them on the basis of the topological properties of the electron density [$\rho(r)$] and its Laplacian [$\nabla^2\rho(r)$] at bond critical points (b.c.p.s) which are located along atomic interaction lines (AILs) or bond paths (Bader & Essén, 1984). Shared-shell covalent interactions are characterized by large positive values of $\rho(r)$ and negative values

of $\nabla^2\rho(r)$, while closed-shell ionic interactions have positive values for both $\rho(r)$ and $\nabla^2\rho(r)$. However, analysis of interactions around heavy atoms in organometallic systems is often more complex owing to the fact that the scattering from core electrons dominates that from valence electrons compared with lighter first-row elements (*e.g.* C, N, O). As a result b.c.p.s are often found in regions of charge depletion [positive values of $\nabla^2\rho(r)$] or missing where chemical intuition would expect them to be present (Farrugia *et al.*, 2006). In view of these issues it is necessary to consider parameters other than just $\rho(r)$ and $\nabla^2\rho(r)$ when examining interactions involving heavy atoms. One approach that has been postulated is to consider the values of the total energy density [$H(\rho)$], the potential energy density [$V(\rho)$] and the kinetic energy density [$G(\rho)$] at the b.c.p.s (Cremer & Kraka, 1984). Shared-shell interactions are defined as having negative values of $H(\rho)$ and $|V(\rho)| > G(\rho)$, while closed-shell interactions have positive values for $H(\rho)$ and $|V(\rho)| < G(\rho)$. A wide range of studies has been carried out classifying bonding on the basis of $H(\rho)$, $V(\rho)$ and $G(\rho)$ values (Macchi *et al.*, 1998*a*; Overgaard *et al.*, 2007). In general more negative values of $H(\rho)$ indicate a greater shared-shell (covalent) interaction, however, this classification does not allow for an intermediate bonding region for example around transition metals. One classification providing such an intermediate bonding region has been suggested based on the value of $|V(\rho)|/G(\rho)$ (Espinosa *et al.*, 2002). Covalent interactions are characterized by negative values of $H(\rho)$ and $|V(\rho)|/G(\rho) > 2$, whilst ionic interactions have positive values of $H(\rho)$ and $|V(\rho)|/G(\rho) < 1$. This leaves an intermediate region which is frequently seen for bonds involving heavy atoms where $H(\rho)$ is negative, indicating some degree of covalency but $1 < |V(\rho)|/G(\rho) < 2$ and in this intermediate region it is more difficult to interpret the interactions correctly. This scheme has been applied successfully in a number of cases including the classification of Mg—Mg bonds in a magnesium dimer (Overgaard *et al.*, 2009). However, there have been several situations cited in which the value of $|V(\rho)|/G(\rho)$ has not provided an adequate description of the nature of the bonding (Gibbs *et al.*, 2006; Gatti & Lasi, 2007). As a result it seems sensible not to consider the value of $|V(\rho)|/G(\rho)$ in isolation.

In organometallic chemistry the bonding between an alkene and late transition metals can be explained using the Chatt–Dewar–Duncanson model. The process can be viewed in two parts, firstly sigma donation of electron density from a filled alkene π orbital donating into a correctly orientated empty metal *d*-orbital, secondly π back-bonding from a filled metal *d*-orbital into the empty antibonding π^* orbital on the alkene. Removing electron density from the alkene-bonding π orbital through sigma donation or increasing electron density in the C═C antibonding π^* orbital through π-back-bonding has the effect of reducing the C═C bond order (*i.e.* weakening the bond) and thus result in a lengthening of the alkene bond. Increasing the level of π-back-bonding increases the C═C bond length and eventually results in the hybridization of the C atoms being reduced from sp^2 to sp^3 forming a metallocyclopropane as opposed to a straighforward alkene adduct. It has been postulated that charge-density analyses of a purely closed-shell alkene–metal adduct would show a T-shaped interaction geometry for the AILs, while a shared-shell covalent metallocyclopropane would have a triangular arrangement of the AILs (Macchi *et al.*, 1998*b*).

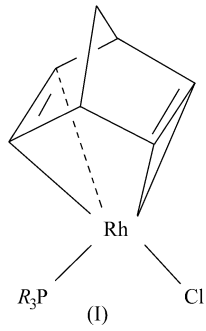

(I)

Complexes of the type $Rh(C_7H_8)(PR_3)Cl$ (R = alkyl or aryl) are useful precursors in the synthesis of intermediate species containing Rh···(C—C) sigma interactions. Given their importance and the difficulty isolating species containing Rh···(C—C) sigma interactions, we have undertaken experimental charge-density studies on two of the precursor species $[Rh(C_7H_8)(P^tBu_3)Cl]$ (1) and $[Rh(C_7H_8)(PCy_3)Cl]$ (2), see (I). Despite the fact that these complexes display Rh–alkene interactions as opposed to Rh···(C—C) sigma interactions, they will provide unique insights into the bonding around rhodium metal centres and serve as an excellent benchmark for more exotic motifs. The results of these studies are presented here and will be compared with our previously published study on $[Rh(C_7H_8)(PPh_3)Cl]$ (Sparkes *et al.*, 2008), with particular attention being given to the bonding around the rhodium metal centre.

2. Experimental

2.1. Synthesis

$Rh(C_7H_8)(PR_3)Cl]$ (R = ^{t}Bu, Cy) were prepared using the method of Chatt & Venanzi (1957; see also Brayshaw *et al.*, 2007). Single crystals suitable for charge-density analysis were obtained by recrystallized from toluene/pentane.

2.2. Data collection and spherical atom refinement

High-resolution single-crystal X-ray diffraction data for both compounds $[Rh(C_7H_8)(P^tBu_3)Cl]$ (1), and $[Rh(C_7H_8)(PCy_3)Cl]$ (2) were collected on an Oxford Diffraction Gemini diffractometer using graphite-monochromated Mo $K\alpha$ radiation (λ = 0.71073 Å) at 100 K. Data were collected and integrated using the *CrysAlis* software (Oxford Diffraction, 2007). Data were subsequently merged using *SORTAV* (Blessing, 1997) within the *WinGX* suite (Farrugia, 1999). The structure was solved using direct methods (*SHELXS*97; Sheldrick, 2008) and refined by full-matrix least squares on F^2 (*SHELXL*97; Sheldrick, 2008). H atoms were located in the difference Fourier map and refined freely. Further details of the experimental data collection and refinement are provided in Table 1.

Table 1
Crystal data and structural refinement details for $[Rh(C_7H_8)(P^tBu_3)Cl]$ (1) and merged data for $[Rh(C_7H_8)(PCy_3)Cl]$ (2).

For all structures: monoclinic, $P2_1/n$, $Z = 4$. Experiments were carried out at 100 K with Mo $K\alpha$ radiation using an Xcalibur, Sapphire3, Gemini ultra diffractometer. Analytical numeric absorption correction using a multifaceted crystal model based on expressions derived by Clark & Reid (1995).

	(1)	(2)
Crystal data		
Empirical formula	$C_{19}H_{35}ClPRh$	$C_{25}H_{41}ClPRh$
M_r	432.80	510.91
a, b, c (Å)	8.4350 (1), 13.9708 (1), 16.6752 (1)	10.2135 (1), 15.8217 (1), 14.6417 (1)
β (°)	103.563 (1)	97.787 (1)
V (Å^3)	1910.26 (2)	2344.21 (3)
μ (mm^{-1})	1.11	0.92
Crystal size (mm)	0.40 × 0.36 × 0.26	0.40 × 0.36 × 0.26
Data collection		
T_{min}, T_{max}	0.717, 0.799	–
No. of measured, independent and observed [$I > 3\sigma(I)$] reflections	198 001, 19 057, 17 131	297 875, 24 737, 21 046
R_{int}	0.029	0.048
R_{merged}	0.029	0.048
Spherical atom refinement		
No. of data in refinement	19 057	20 004
No. of refined parameters	339	417
GOF (F^2)	0.944	1.012
Final R_1 [$F^2 > 2\sigma(F)$] (all data)	0.0154 (0.0226)	0.0213 (0.0297)
wR_2 [$F^2 > 2\sigma(F)$] (all data)	0.0367 (0.0375)	0.0481 (0.0500)
$\Delta\rho_{max}$, $\Delta\rho_{min}$ (e Å^{-3})	0.83, −0.74	0.79, −0.61
Multipole refinement		
No. of data in refinement (N_{ref})	16 456	18 953
No. of refined parameters (N_v)	430	517
GOF (F)	1.30	1.23
N_{ref}/N_v	38.27	36.66
Final R_1 [$I > 3\sigma(I)$] (all data)	0.0124 (0.0190)	0.0156 (0.0282)
wR_2 [$I > 3\sigma(I)$]	0.0114	0.0132
$\Delta\rho_{max}$, $\Delta\rho_{min}$ (e Å^{-3})	0.32, −0.40	0.41, −0.39

Computer programs used: *CrysAlisPro* (Oxford Diffraction, 2007), *SHELXS*97 (Sheldrick, 2008), *XD*2006 (Volkov *et al.*, 2006).

2.2.1. Specific details for $[Rh(C_7H_8)(P^tBu_3)Cl]$ (1). 198 001 measured reflections were merged to give 19 057 unique reflections, with a merging R factor of 0.029; 5 reflections were missing up to $\sin\theta/\lambda = 1.06$ Å^{-1}. A plot of scale factor *versus* resolution for the dataset was satisfactory with a maximum variation of ± 3% around unity, see Fig. S1 of the supplementary material.[1]

2.2.2. Specific details for $[Rh(C_7H_8)(PCy_3)Cl]$ (2). Two high-resolution datasets were collected from two different crystals (see Table S1 in the supplementary information). Both datasets were from good crystals, but for the second, the high-angle data were much weaker. The redundancy was low (approximately fivefold) for both datasets and hence they were merged. The datasets were scaled together using *SORTAV* giving 297 875 reflections which were subsequently merged to give 24 737 unique reflections, with a merging R factor of 0.048; 3 reflections were missing up to $\sin\theta/\lambda = 1.06$ Å^{-1}. A plot of the scale factor *versus* resolution for the dataset was satisfactory with a maximum variation of ±3% around unity, see Fig. S1.

2.3. Multipole refinement

Aspherical atom refinements were carried out using *XD*2006 (Volkov *et al.*, 2006) using the spherical atom models obtained from refinement in *SHELXL* (Sheldrick, 2008) as starting points. *XD*2006 implements the multipole formalism of Hansen & Coppens (1978). For both compounds the presence of a second-row transition metal (Rh) means that relativistic effects will be significant and must be accounted for since excluding them affects the accuracy of the topological properties at critical points (Eickerling *et al.*, 2007). With this taken into account all of the appropriate databanks available in *XD*2006 were tested in order to obtain the best refinement; although the results were similar, STO-Dirac-Fock atomic relativistic wavefunctions (Su & Coppens, 1998; Macchi & Coppens, 2001) gave a slightly better refinement and hence were used in the final refinements for both compounds. A similar general refinement strategy was followed for both (1) and (2); the electronic configuration $5s^14d^8$ was used for rhodium with the $5s^1$ scattering contribution fixed as part of the core contribution. Initially only the scale factor was refined, followed by the atomic positions and displacement parameters. Subsequently, a high-order refinement ($\sin\theta/\lambda >$ 0.7 Å^{-1}) was carried out to determine the optimal atomic positions and displacement parameters for the non-H atoms. This was followed by a low-order refinement ($\sin\theta/\lambda <$ 0.7 Å^{-1}) of the positional and isotropic displacement parameters of the H atoms; once this refinement reached convergence the isotropic displacement parameters for the H atoms were fixed for the remainder of the refinements. In all further refinement cycles, the C—H bond lengths were reset to their average neutron diffraction distances of 1.06 Å (methyl) and 1.10 Å (cage H and Cy groups). The multipole expansion was truncated at the hexadecapole level for rhodium, phosphorus and chlorine, the octupole level for all C atoms and the bond-directed dipole level for the H atoms. The charge on the complex was maintained throughout the refinement using the

[1] Supplementary data for this paper are available from the IUCr electronic archives (Reference: SO5039). Services for accessing these data are described at the back of the journal.

command KEEP charge group 1. Five κ parameters were refined for all atom types along with four κ' parameters for the non-H atoms, the κ' parameters were constrained to be the same for all multipoles. At the end of the multipole refinement a plot of scale factor *versus* resolution for the dataset was satisfactory with a maximum variation of $< \pm 3\%$ around unity, see Fig. S2. The energy densities at the b.c.p.s, after completion of the multipole refinement, were derived using the Abramov approximation implemented in *WinXPRO* (Abramov, 1997).

2.3.1. Specific details for [Rh(C_7H_8)(P^tBu_3)Cl] (1). During the refinement, the H atoms were assigned to four groups (methyl, methylene, vinyl and those attached to C3/C6), while the C atoms of the tertiary butyl groups were assigned to two groups depending on their type, the valence deformation density for each group of atoms was constrained to be the same using the CHEMCON constraint in *XD*2006. Inclusion of an isotropic extinction coefficient produced a small but significant improvement in the refinement and hence was included in the final refinement. The residual density map at the end of this stage of the refinement had sharp peaks near the Cl atom, suggesting evidence of anharmonicity for the Cl atom, and the inclusion of third-order Gram–Charlier coefficients produced a significant improvement in the refinement [$R(F)$ = 0.0128, GOF = 1.35 before compared with $R(F)$ = 0.0124, GOF = 1.30 after inclusion]. Data collections at higher temperatures showed larger peaks near the chlorine supporting the assertion of anharmonicity. The residual density map, at the end of the refinement using all data, was almost featureless with maximum residuals of 0.32 and -0.40 e Å^{-3}, which as expected were near the Rh atom, see Fig. S3. The Hirshfeld rigid-bond test (Hirshfeld, 1976) was carried out after the multipole refinement was deemed to be satisfactory (Table S2). All the Rh—C bonds had significantly higher maximum mean-square atomic displacements along the bond directions (22–23 $\times 10^{-4}$ Å^2) than found for the rest of the bonds in the complex, for which the next highest value was 16×10^{-4} Å^2 for Rh1—Cl1; this is due to the fact that the Hirshfeld test is typically applied to atoms with similar masses and for these bonds there are large differences in the atomic masses of the atoms involved. The integrated Bader charge for Rh1 was 0.30 Ω. Further details of the refinement results are provided in Table 1.

2.3.2. Specific details for [Rh(C_7H_8)(PCy_3)Cl] (2). The valence deformation densities of five groups of H atoms [methylene (cage and cyclohexyl), vinyl, those attached to C3/C6 and those attached to C8/C14/C20], and four groups of cyclohexyl C atoms (assigned depending on their location around the ring) were constrained to be the same using the CHEMCON constraint in *XD*2006. At the end of the refinement, the residual density map was almost featureless with maximum residuals of 0.41 and -0.39 e Å^{-3}, see Fig. S4, and the Hirshfeld rigid-bond test was satisfactory (Table S3). As seen for (1) all of the Rh—C bonds had significantly higher maximum mean-square atomic displacement parameters along the bond directions (18–24 $\times 10^{-4}$ Å^2). The integrated Bader charge for Rh1 was 0.49 Ω. Further details of the refinement results are provided in Table 1.

3. Results and discussion

Scheme (I) shows the two compounds under study: [Rh(C_7H_8)(P^tBu_3)Cl] (1) and [Rh(C_7H_8)(PCy_3)Cl] (2). The structures of the complexes are very similar and both have an approximately square-planar rhodium metal centre with a formal charge of +1 surrounded by a norbornadiene cage, chloride ligand and phosphine ligand. The only difference between the species is the nature of the phosphine ligand: P^tBu_3 in the case of (1) and PCy_3 in the case of (2). Details of the data collection and subsequent charge-density analysis are provided in Table 1.

3.1. [Rh(C_7H_8)(P^tBu_3)Cl] (1)

An *ORTEP* plot of (1) provided in Fig. 1 illustrates the numbering scheme used. The topological properties for selected b.c.p.s are provided in Table 2. The topological parameters for the C—C bonds in the tertiary butyl fragments are as expected, consistent with them being single shared-shell covalent interactions, with large positive values of $\rho(r)$ (1.54–1.59 e Å^{-3}), negative values of $\nabla^2\rho(r)$ (-7.14 to -7.88 e Å^{-5}), C—C bond lengths (d_{ij}) of $\sim$ 1.54 Å and small ellipticities (ϵ) ranging from 0.01 to 0.05. The P—C bonds are also unremarkable with $\rho(r)$ ranging from 0.96 to 1.01 e Å^{-3} and negative values for its Laplacian ranging from -3.41 to -4.19 e Å^{-5} at the b.c.p.s. The values of $\rho(r)$ and negative values of the Laplacian of $\rho(r)$, combined with relatively small ellipticity values (0.03–0.08) again indicate these bonds to be covalent single bonds.

If we examine the bonding around rhodium it can be seen that a b.c.p. was identified between both Rh—P and Rh—Cl. Using simple topological considerations these would be characterized as closed-shell ionic interactions owing to their small positive values of $\rho(r)$ and $\nabla^2\rho(r)$. However, as mentioned previously such a simple analysis is not suitable for bonding around heavy elements, and it is necessary to consider

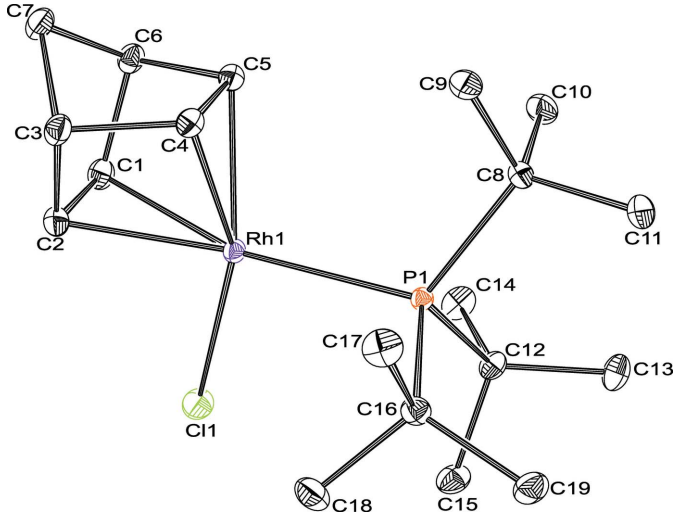

Figure 1
ORTEP plot for [Rh(C_7H_8)(P^tBu_3)Cl] (1) at 100 K, with ellipsoids depicted at the 50% level. H atoms are omitted for clarity.

Table 2
Topological properties at the b.c.p.s in [Rh(C_7H_8)(P^tBu_3)Cl] (1).

Bond	d_{ij} (Å)	R_{ij} (Å)†	$\rho(r_{bcp})$ (e Å^{-3})	$\nabla^2\rho(r_{bcp})$ (e Å^{-5})	$H(\rho)$ (a.u.)	$G(\rho)$ (a.u.)	$V(\rho)$ (a.u.)	$\lvert V(\rho)\rvert/G(\rho)$ (a.u.)	ϵ
Rh1—C1	2.1911 (3)	–	–	–	–	–	–	–	–
Rh1—C2	2.1846 (3)	2.2626	0.59 (1)	6.38 (1)	−0.028	0.093	−0.121	1.299	13.14
Rh1—C4	2.1113 (3)	–	–	–	–	–	–	–	–
Rh1—C5	2.1117 (3)	2.1359	0.66 (1)	6.73 (1)	−0.038	0.107	−0.145	1.359	2.03
Rh1—P1	2.4334 (1)	2.4336	0.55 (1)	3.58 (1)	−0.032	0.068	−0.101	1.474	0.10
Rh1—Cl1	2.3895 (1)	2.3901	0.43 (1)	5.75 (1)	−0.010	0.069	−0.078	1.140	0.07
P1—C8	1.9245 (3)	1.9245	0.96 (1)	−3.41 (2)	−0.122	0.087	−0.209	2.408	0.06
P1—C12	1.9211 (3)	1.9218	0.97 (1)	−3.66 (2)	−0.127	0.089	−0.215	2.429	0.08
P1—C16	1.9107 (3)	1.9107	1.01 (1)	−4.19 (2)	−0.136	0.092	−0.228	2.471	0.03
C1—C2	1.3919 (5)	1.3930	2.12 (2)	−16.34 (5)	−0.472	0.303	−0.775	2.560	0.36
C1—C6	1.5381 (6)	1.5393	1.57 (2)	−7.79 (3)	−0.280	0.200	−0.480	2.405	0.09
C2—C3	1.5386 (5)	1.5406	1.57 (2)	−8.18 (3)	−0.281	0.196	−0.478	2.432	0.10
C3—C4	1.5379 (5)	1.5383	1.62 (2)	−7.97 (3)	−0.292	0.209	−0.502	2.395	0.04
C3—C7	1.5455 (5)	1.5457	1.56 (2)	−7.96 (3)	−0.276	0.194	−0.470	2.426	0.09
C4—C5	1.4188 (5)	1.4198	1.96 (2)	−11.95 (4)	−0.406	0.282	−0.689	2.439	0.31
C5—C6	1.5390 (5)	1.5403	1.62 (2)	−8.54 (3)	−0.296	0.207	−0.503	2.428	0.07
C6—C7	1.5447 (5)	1.5452	1.56 (2)	−7.63 (3)	−0.276	0.196	−0.472	2.403	0.03
C8—C9	1.5460 (5)	1.5465	1.54 (1)	−7.14 (2)	−0.269	0.195	−0.465	2.379	0.01
C8—C10	1.5444 (4)	1.5447	1.56 (1)	−7.48 (2)	−0.276	0.198	−0.474	2.391	0.03
C8—C11	1.5421 (4)	1.5426	1.58 (1)	−7.69 (2)	−0.283	0.203	−0.485	2.393	0.03
C12—C13	1.5407 (5)	1.5415	1.58 (1)	−7.62 (2)	−0.282	0.203	−0.485	2.390	0.04
C12—C14	1.5449 (5)	1.5455	1.55 (1)	−7.31 (2)	−0.272	0.196	−0.468	2.387	0.05
C12—C15	1.5416 (5)	1.5420	1.55 (1)	−7.19 (2)	−0.271	0.196	−0.467	2.380	0.03
C16—C17	1.5411 (5)	1.5411	1.59 (1)	−7.88 (2)	−0.286	0.205	−0.491	2.400	0.02
C16—C18	1.5415 (4)	1.5426	1.57 (1)	−7.64 (2)	−0.278	0.199	−0.478	2.398	0.02
C16—C19	1.5412 (5)	1.5414	1.56 (1)	−7.44 (2)	−0.274	0.197	−0.472	2.391	0.01
C—H‡ (vinyl)	1.10	1.10	1.79 (2)	−16.76 (5)	–	–	–	–	0.04
C—H‡ (H3/H6)	1.10	1.10	1.77 (2)	−15.40 (7)	–	–	–	–	0.02
C—H‡ (methylene)	1.10	1.10	1.77 (2)	−15.26 (6)	–	–	–	–	0.03
C—H‡ (methyl)	1.08	1.08	1.77 (1)	−14.26 (2)	–	–	–	–	0.03

† R_{ij} is the length of the bond path between the two atoms i and j. ‡ Average values for C—H bonds of the type specified.

the energetics of the interactions, see Table 2. In both cases the values of the total energy density $H(\rho)$ have a small negative value and $|V(\rho)| > G(\rho)$, indicating some degree of covalency, while the value of $|V(\rho)|/G(\rho)$ lies between 1 and 2, thus suggesting that the bonds fall in the intermediate bonding region somewhere between a pure shared-shell covalent and a closed-shell ionic description. The more negative value of $H(\rho)$, combined with a larger $|V(\rho)|/G(\rho)$ value for the Rh1—P1 interaction than for the Rh1—Cl1 interaction, suggests that the former interaction is more covalent in nature and the latter more ionic in nature, which fits from a chemical perspective. When examining plots of the Laplacian of the electron density the presence of a charge concentration between atoms in the plane of the plot implies that there is an interaction between the atoms, while the magnitude of the charge concentration indicates the degree of covalency (*i.e.* a region of charge concentration). A plot of the Laplacian of $\rho(r)$ in the Rh1—P1—Cl1 plane shows evidence of a charge concentration at both P1 and Cl1 directed towards Rh1, albeit much smaller on the almost spherical Cl atom, see Fig. 2. This indicates that as anticipated from the energetic parameters both P1 and Cl1 interact with rhodium, and the Rh1—P1 interaction is more covalent in nature than the Rh1—Cl1 interaction. This is supported by the fact that the deformation density map also shows clear evidence of electron density from both atoms directed towards rhodium, see Fig. 3.

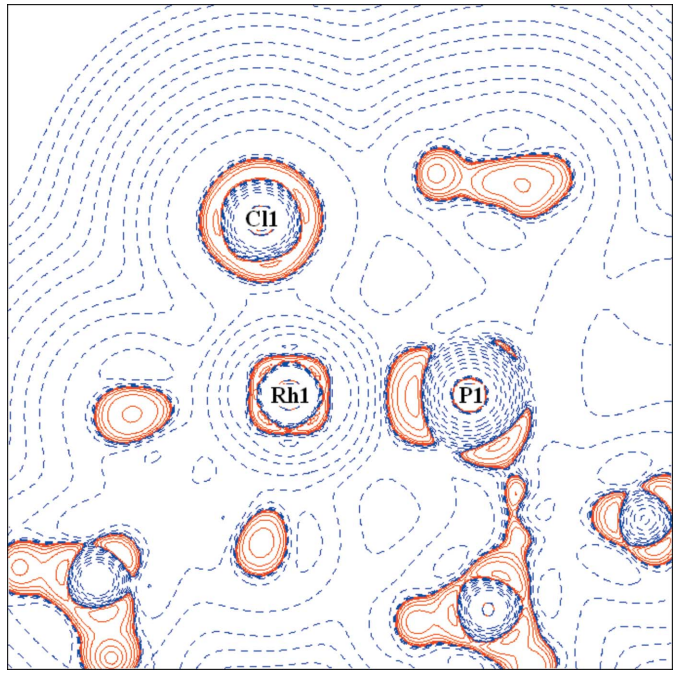

Figure 2
Negative Laplacian of the electron density for [Rh(C_7H_8)(P^tBu_3)Cl] (1), drawn in the Rh1—P1—Cl1 plane, with positive contours as solid red lines and negative contours as dashed blue lines.

The topological analysis of the charge density in the norbornadiene fragment indicates that the C—C bonding is covalent in nature [large positive values of $\rho(r)$ and negative values of the Laplacian of $\rho(r)$]. The formally single C—C bonds in the fragment have $\rho(r)$ values ranging from 1.56 to 1.62 e Å^{-3} and negative values for the Laplacian ranging from −7.63 to −8.54 e Å^{-5}. The increased electron density in the carbon double bonds, C1═C2 and C4═C5, compared with single bonds is reflected in larger values for $\rho(r)$ (2.12 and 1.96 e Å^{-3} respectively) and the Laplacian of $\rho(r)$ (−16.34 and −11.95 e Å^{-5}, respectively) at their b.c.p.s. As expected, the ellipticities for the single C—C bonds (0.03–0.10) are considerably lower than those for the double C—C bonds (0.31–0.36). Variations in the topological parameters for the double bonds are significant and indicate differences between the two ends of the norbornadiene cage. The C4═C5 bond appears to be weaker than the C1═C2 bond with lower values of $\rho(r)$ and $\nabla^2\rho(r)$ at the b.c.p. and an ∼ 0.03 Å longer bond length. In addition, it is noteworthy that the $M—L$ bond lengths to C1/C2 are ∼ 0.07 Å longer than those to C4/C5. These variations were expected as the phosphorus ligand has a stronger *trans* influence than chlorine and therefore weakens $M—L$ bonds *trans* to it resulting in a stronger C═C bond *trans* to phosphorus.

In terms of bonding between rhodium and the four C atoms of the cage (C1, C2, C4 and C5) only two of the expected four b.c.p.s were identified; those between Rh1—C1 and Rh1—C4 were absent despite having similar atom separations to Rh1—C2 and Rh1—C5. However, as mentioned in §1 the bonding involving heavy atoms such as rhodium can be far more complex to analyse and understand than that for purely organic species, hence it is worth looking in more detail at this bonding. Beginning by examining the parameters in Table 2 associated with the two located Rh—C b.c.p.s (Rh1—C2 and Rh1—C5), it can be seen that there are small positive values for ρ, positive values for the Laplacian of ρ, small negative values for the total energy density [$H(\rho)$], $|V(\rho)| > G(\rho)$ and a $|V(\rho)|/G(\rho)$ value between 1 and 2. All of these points indicate that, as seen for the other bonds involving rhodium, the bonding contains some degree of covalency. The larger magnitudes of ρ, $\nabla^2\rho(r)$, $H(\rho)$ and $|V(\rho)|/G(\rho)$ for the Rh1—C5 interaction compared with the Rh1—C2 interaction indicate that the former interaction is slightly stronger and more covalent than the latter, which is likely to be due to the *trans* influence of phosphorus weakening the Rh1—C2 interaction. It is noteworthy at this point that the bond paths for the Rh—C interactions are significantly longer than the separation of the atoms [Rh1—C2, R_{ij} = 2.2626 Å, d_{ij} = 2.1846 (3) Å; Rh1—C5, R_{ij} = 2.1359 Å, d_{ij} = 2.1117 (3) Å], which indicates that the bond paths are curved.

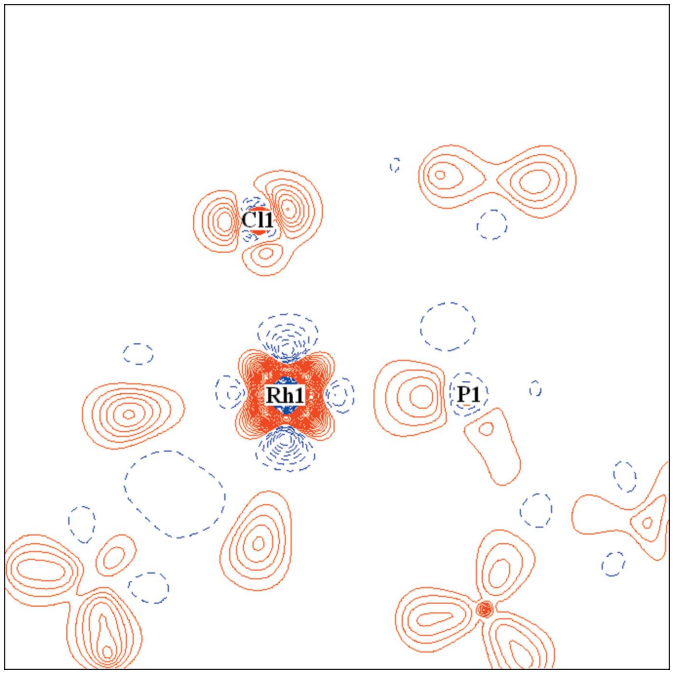

Figure 3
Deformation density map for [Rh(C_7H_8)(P^{t}Bu$_3$)Cl] (1), after multipole refinement drawn in the plane of Rh1—P1—Cl1. Contours are depicted at the 0.1 e Å^{-3} level, with positive contours as solid red lines and negative contours as blue dashed lines. The zero line is omitted.

It is now worth investigating whether the absence of two b.c.p.s (those between Rh1—C1 and Rh1—C4) suggests that these two C atoms are not involved in bonding to rhodium, despite the fact that their atomic separations are similar to those for Rh1—C2 and Rh1—C5. Examining the plots of the Laplacian of the electron density between rhodium and the cage C atoms shown in Fig. 4 shows clear evidence of charge concentrations at all four C atoms directed towards rhodium. In addition, Fig. 5 shows that there is clear evidence of a distortion of the electron density in both the C1═C2 and C4═C5 bonds towards rhodium, which is supported by the high ellipticities of these bonds (0.36 and 0.31). Based on this it seems reasonable to suggest that all four of the expected C atoms (C1, C2, C4 and C5) are involved in bonding to rhodium. The reasons for the absence of the two b.c.p.s will now be examined. As can be seen from Fig. 6, the bond paths for both Rh—C2 and Rh—C5 are curved, the former more than the latter, with the location of the b.c.p. approaching the area where a ring critical point (r.c.p.) might have been expected. The [λ_1, λ_2, λ_3] eigenvalues associated with the Rh1—C2 bond [−2.47, −0.17, 9.02] and those with the Rh1—C5 bond [−2.82, −0.93, 10.48] have very small values for λ_2, indicating that the electron density is very flat in one direction perpendicular to the bond path, *i.e.* in the region between rhodium and the two C═C bonds, see Fig. S5. In a recent charge-density analysis of a Co dimer containing alkene fragments (Overgaard *et al.*, 2008), it was noted that the electron density was very flat near the centre of the CoC_2 triangles. Given that this region is where the b.c.p.s and the r.c.p. would be expected, only a small change in the electron density could cause b.c.p.s and r.c.p.s to coalesce in a bond catastrophe (Bader, 1990). The occurrence of a bond catastrophe at one end of the norbornadiene cage was also seen for [Rh(C_7H_8)(PPh_3)Cl] (Sparkes *et al.*, 2008) and given the evidence that all four C atoms in the current study are involved in bonding to rhodium, it seems reasonable that the

flat electron density and curved bond paths have resulted in a bond catastrophe occurring.

As discussed earlier, the nature of the bonding between an alkene and a transition metal affects the geometry of the AILs in a charge-density analysis. For a purely closed-shell interaction a T-shaped geometry is expected while a covalent metallocyclopropane would be triangular. The T-shaped alkene adduct has been observed in $[Ag(\eta^2\text{-}C_2H_2)][Al(OC(CH_3)(CF_3)_2)_4]$ (Reisinger *et al.*, 2007). However, it is rare to see either of these two extremes and far more common to see an intermediate situation, with evidence for the presence of both sigma donation and π-backbonding gained from the nature of the AILs. Sigma donation results in concave bond paths arising from the presence of a charge concentration in the $M-C{=}C$ triangle, while increased π back-donation causes a widening of the $M-C$ AILs (Macchi *et al.*, 1998*b*). In a comparison of the experimental charge-density analyses of $[Ni(\eta^2\text{-}C_2H_4)dbpe]$ with the computational

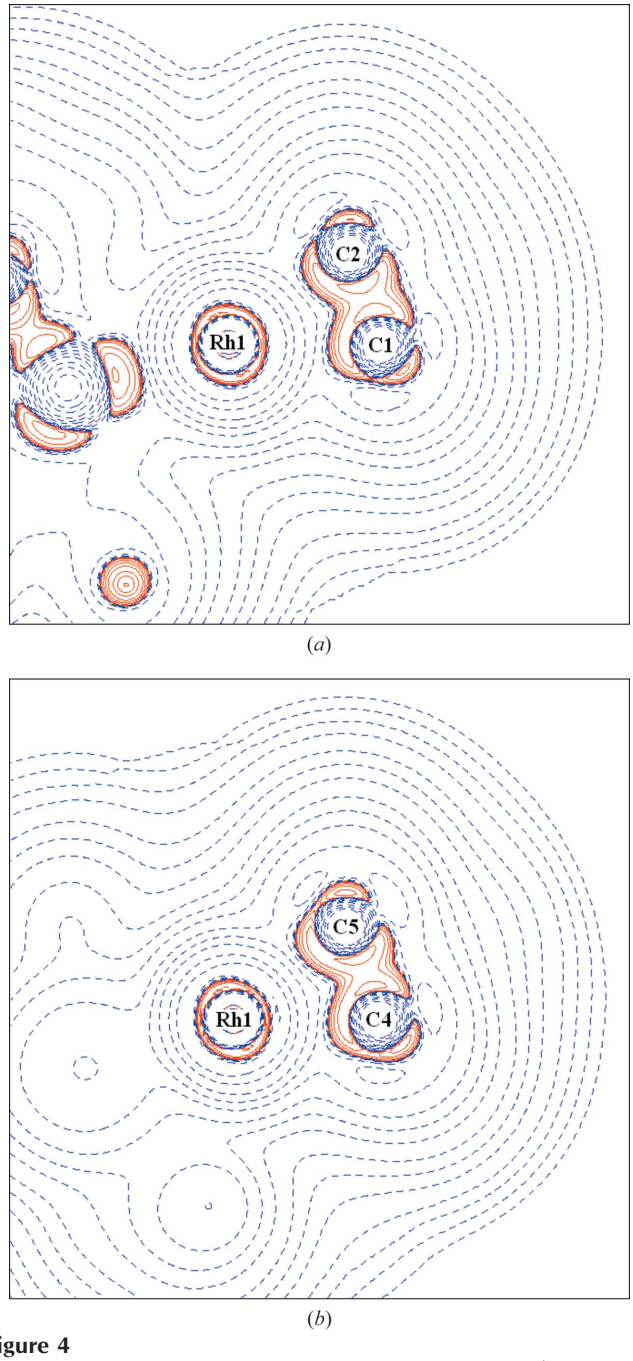

Figure 4
Negative Laplacian of the electron density for $[Rh(C_7H_8)(P^tBu_3)Cl]$ (1), drawn in (*a*) the Rh1—C1—C2 plane and (*b*) Rh1—C4—C5, with positive contours as solid red lines and negative contours as dashed blue lines.

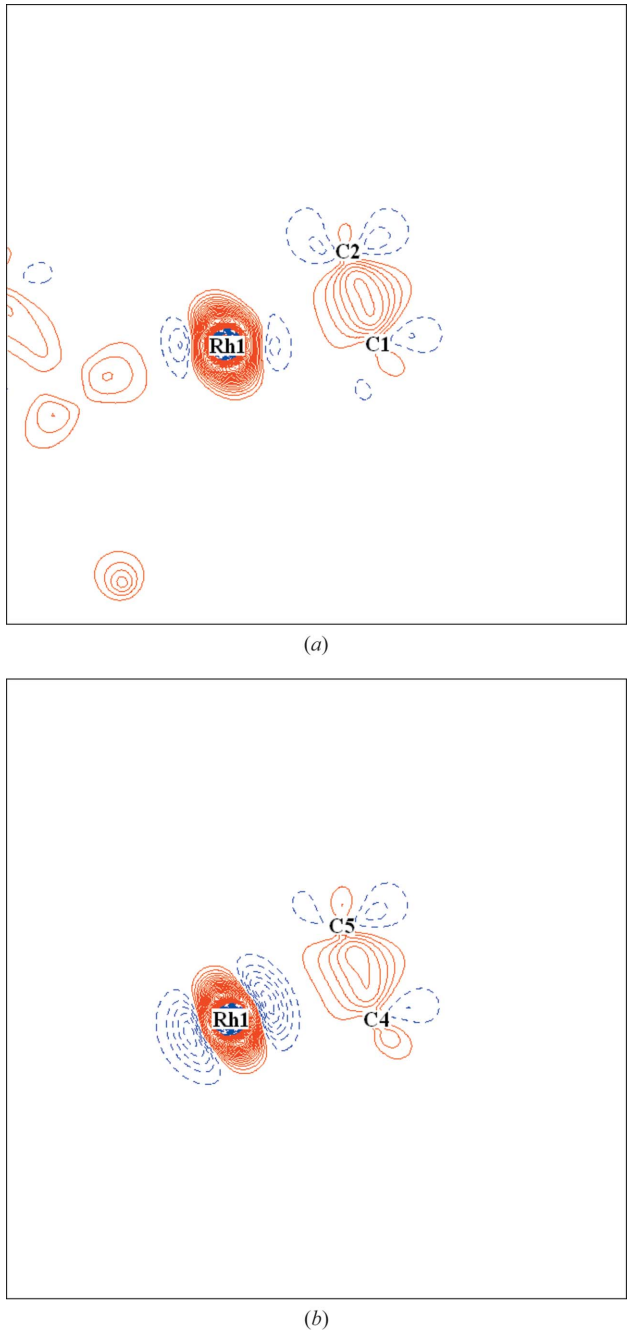

Figure 5
Deformation density map for $[Rh(C_7H_8)(P^tBu_3)Cl]$ (1), after multipole refinement drawn in (*a*) the Rh1—C1—C2 plane and (*b*) Rh1—C4—C5. Contours are depicted at the 0.1 e $Å^{-3}$ level, with positive contours as solid red lines and negative contours as blue dashed lines.

results for [Ni(η^2-C_2H_4)TMEDA] and [Ni(η^2-C_2F_4)TMEDA] it was noted that the situation was slightly more complex. As the carbon hybridization became more sp^3-like, the 'alkene' carbon charge concentrations directed towards Ni increased and the Ni—C AIL became more exocyclic near the C atom, *i.e.* displaced towards the carbon charge concentration (Scherer *et al.*, 2006). Although we only have one Rh—C b.c.p. associated with each end of the norbornadiene cage, we have already established that all four C atoms appear to be involved in bonding to rhodium, hence we will consider how the two Rh—C═C interactions seem to differ. Examining Fig. 6 shows a distinct concave curvature to the two identified Rh—C bond paths which would not be consistent with the expected interaction geometry for an ideal metallocyclopropane or an ionic T-shaped interaction. These assertions are confirmed by the fact that the interactions show a degree of covalency which has been identified on the basis of the energetic parameters of the interaction. On the basis of the concave bond paths the presence of sigma donation can be inferred in both cases, however, the extent of the curvature is different in both cases which is likely to indicate differences in the extent of the π back-bonding. In the case of the Rh1—C2 interaction the bond path is significantly more curved than the Rh1—C5 bond path, with the Rh1—C2 bond path being 0.078 Å longer than the separation of the atoms compared with a difference of 0.024 Å for Rh1—C5. This suggests that there is more π back-bonding between Rh1—C5 than Rh1—C2. This would be expected as a result of the greater *trans*-influence of phosphorus compared with chlorine weakening the Rh—C bonds *trans* to it. Indeed, the *trans* influence of phosphorus has already been shown on the basis of differences in the topological and geometrical properties associated with bonding between rhodium and the two ends of the norbornadiene cage, which indicate that the Rh1—C5 bond is stronger than the Rh1—C2 bond and concomitantly the C1═C2 bond is stronger than the C4═C5 bond.

3.2. [Rh(C_7H_8)(PCy_3)Cl] (2)

An *ORTEP* plot of (2) is provided in Fig. 7. Given the similarities of complexes (1) and (2), it is not necessary to discuss the results of the charge-density analysis for (2) in the same detail and only the key points will be summarized here. The topological properties of selected b.c.p.s are listed in Table 3.

The topological parameters associated with the cyclohexyl C—C bonds have similar values to those seen for the single C—C bonds in (1) and are, as expected, consistent with their being covalent single bonds, with values of $\rho(r)$ (1.57–1.65 e Å^{-3}), $\nabla^2\rho(r)$ (−7.47 to −8.53 e Å^{-5}), C—C bond lengths of around ∼1.53 Å, and small ellipticity values ranging from 0.01 to 0.04. The P—C bonds also have topological parameters in line with those that would be expected for single shared-shell covalent interactions with $\rho(r)$ ranging from 1.11 to 1.13 e Å^{-3}, negative values for its Laplacian ranging from −5.30 to −5.46 e Å^{-5} and small ellipticity values of 0.03–0.08. Similarly the topological parameters for the norbornadiene are comparable to those seen in (1), with the C—C single bonds having values of $\rho(r)$ (1.51–1.64 e Å^{-3}) and negative values for the Laplacian (−6.25 to −8.20 e Å^{-5}) at the b.c.p.s. Again the smaller magnitude of the values for the topological parameters of the C4═C5 b.c.p. [$\rho(r)$ = 1.94 e Å^{-3}, $\nabla^2\rho(r)$ = −10.93 e Å^{-5}] compared with the C1═C2 b.c.p. [$\rho(r)$ = 2.11 e Å^{-3}, $\nabla^2\rho(r)$ = −15.65 e Å^{-5}]

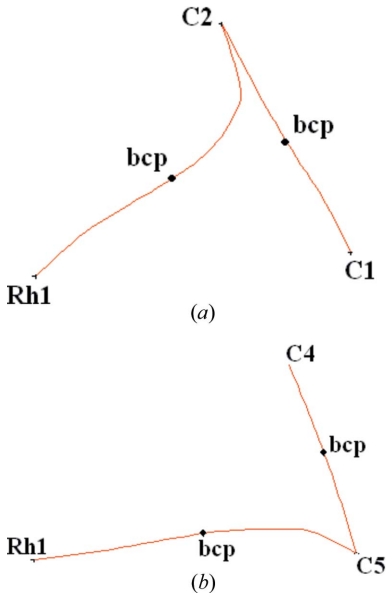

Figure 6
Bond paths in [Rh(C_7H_8)(P^tBu_3)Cl] (1) between rhodium and the norbornadiene cage with b.c.p.s marked for (*a*) Rh1—C1—C2 and (*b*) Rh—C4—C5.

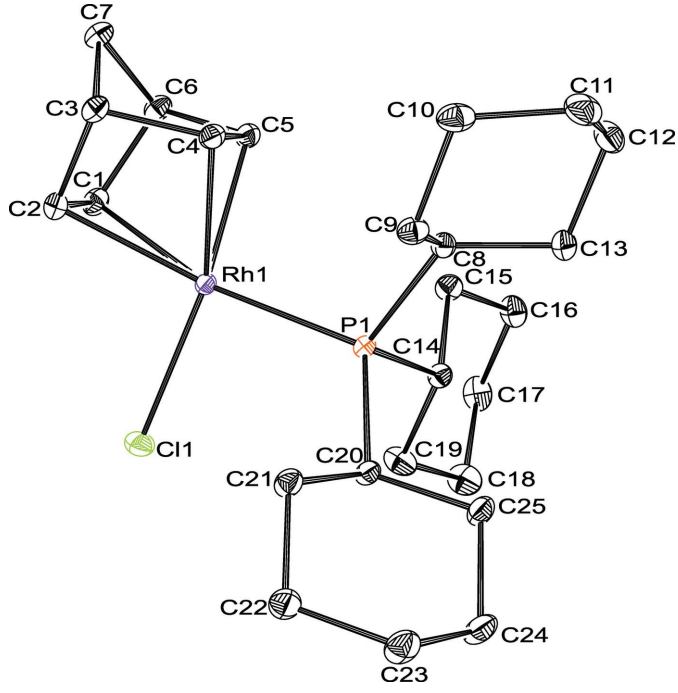

Figure 7
ORTEP plot for [Rh(C_7H_8)(PCy_3)Cl] (2) at 100 K with ellipsoids depicted at the 50% level. H atoms are omitted for clarity.

Table 3
Topological properties at the b.c.p.s in [Rh(C_7H_8)(PCy_3)Cl] (2).

Bond	d_{ij} (Å)	R_{ij} (Å)†	$\rho(r_{bcp})$ (e Å^{-3})	$\nabla^2\rho(r_{bcp})$ (e Å^{-5})	$H(\rho)$ (a.u.)	$G(\rho)$ (a.u.)	$V(\rho)$ (a.u.)	$\lvert V(\rho)\rvert/G(\rho)$ (a.u.)	ϵ
Rh1—C1	2.2330 (4)	2.3107	0.51 (1)	6.06 (1)	−0.019	0.081	−0.101	1.240	7.59
Rh1—C2	2.2201 (4)	–	–	–	–	–	–	–	–
Rh1—C4	2.1019 (4)	2.1199	0.71 (1)	7.60 (1)	−0.043	0.120	−0.163	1.358	1.47
Rh1—C5	2.1091 (4)	–	–	–	–	–	–	–	–
Rh1—P1	2.3160 (1)	2.3164	0.64 (1)	4.86 (1)	−0.043	0.091	−0.134	1.470	0.13
Rh1—Cl1	2.3469 (1)	2.3470	0.47 (1)	7.03 (1)	−0.011	0.083	−0.094	1.134	0.13
P1—C8	1.8561 (4)	1.8570	1.13 (2)	−5.46 (3)	−0.165	0.108	−0.273	2.523	0.03
P1—C14	1.8522 (4)	1.8535	1.11 (2)	−5.30 (4)	−0.159	0.104	−0.264	2.527	0.08
P1—C20	1.8547 (4)	1.8550	1.12 (2)	−5.32 (3)	−0.161	0.106	−0.267	2.520	0.04
C1—C2	1.3847 (7)	1.3864	2.11 (3)	−15.65 (7)	−0.470	0.306	−0.775	2.530	0.43
C1—C6	1.5401 (7)	1.5417	1.62 (2)	−7.68 (4)	−0.291	0.212	−0.503	2.377	0.15
C2—C3	1.5408 (6)	1.5433	1.64 (2)	−7.89 (4)	−0.297	0.216	−0.513	2.380	0.10
C3—C4	1.5418 (6)	1.5426	1.64 (2)	−8.20 (4)	−0.298	0.213	−0.510	2.400	0.07
C3—C7	1.5470 (6)	1.5479	1.51 (2)	−6.25 (4)	−0.257	0.193	−0.450	2.337	0.03
C4—C5	1.4177 (6)	1.4189	1.94 (2)	−10.93 (6)	−0.396	0.283	−0.679	2.400	0.57
C5—C6	1.5445 (6)	1.5455	1.53 (2)	−6.56 (4)	−0.263	0.195	−0.458	2.349	0.16
C6—C7	1.5483 (6)	1.5492	1.56 (2)	−7.15 (4)	−0.276	0.201	−0.477	2.368	0.04
C8—C9	1.5396 (5)	1.5397	1.57 (1)	−7.47 (2)	−0.280	0.202	−0.482	2.383	0.02
C8—C13	1.5380 (5)	1.5383	1.58 (1)	−7.61 (2)	−0.282	0.203	−0.485	2.389	0.02
C9—C10	1.5294 (6)	1.5294	1.63 (1)	−8.32 (2)	−0.297	0.211	−0.508	2.409	0.04
C10—C11	1.5303 (7)	1.5304	1.59 (1)	−7.78 (3)	−0.286	0.205	−0.490	2.394	0.03
C11—C12	1.5344 (7)	1.5345	1.63 (1)	−8.22 (2)	−0.297	0.212	−0.509	2.403	0.04
C12—C13	1.5384 (6)	1.5385	1.61 (1)	−7.96 (2)	−0.291	0.209	−0.500	2.396	0.03
C14—C15	1.5334 (5)	1.5334	1.60 (1)	−7.86 (2)	−0.289	0.207	−0.496	2.393	0.01
C14—C19	1.5346 (6)	1.5346	1.59 (1)	−7.69 (2)	−0.284	0.204	−0.488	2.391	0.02
C15—C16	1.5315 (6)	1.5315	1.62 (1)	−8.28 (2)	−0.296	0.210	−0.506	2.409	0.01
C16—C17	1.5269 (7)	1.5269	1.65 (1)	−8.53 (2)	−0.304	0.215	−0.519	2.412	0.04
C17—C18	1.5294 (7)	1.5294	1.62 (1)	−8.08 (2)	−0.293	0.209	−0.502	2.400	0.04
C18—C19	1.5318 (6)	1.5319	1.60 (1)	−8.01 (2)	−0.289	0.206	−0.495	2.404	0.04
C20—C21	1.5370 (5)	1.5371	1.59 (1)	−7.67 (2)	−0.285	0.205	−0.490	2.387	0.01
C20—C25	1.5363 (5)	1.5363	1.58 (1)	−7.65 (2)	−0.282	0.203	−0.485	2.391	0.02
C21—C22	1.5327 (5)	1.5328	1.62 (1)	−8.21 (2)	−0.295	0.210	−0.504	2.406	0.02
C22—C23	1.5291 (6)	1.5291	1.64 (1)	−8.48 (2)	−0.302	0.214	−0.516	2.411	0.03
C23—C24	1.5276 (6)	1.5277	1.60 (1)	−7.90 (2)	−0.288	0.206	−0.494	2.398	0.04
C24—C25	1.5324 (6)	1.5325	1.62 (1)	−8.25 (2)	−0.295	0.210	−0.505	2.408	0.02
C—H‡ (vinyl)	1.10	1.10	1.82 (2)	−17.93 (5)	–	–	–	–	0.05
C—H‡ (H3/H6)	1.10	1.10	1.80 (3)	−15.92 (7)	–	–	–	–	0.01
C—H‡ (methylene, cage)	1.10	1.10	1.81 (3)	−15.54 (7)	–	–	–	–	0.04
C—H‡ (methylene, cyclohexyl)	1.10	1.10	1.74 (2)	−13.82 (3)	–	–	–	–	0.02
C—H‡ (H8/H14/H20)	1.10	1.10	1.74 (2)	−13.48 (6)	–	–	–	–	0.01

† R_{ij} is the length of the bond path between two atoms i and j. ‡ Average values for C—H bonds of the type specified.

indicate that the C4═C5 bond is weaker than the C1═C2 bond. Given that the M—L bond distances are longer between Rh1 and C1/C2 compared with those from Rh1 to C4/C5, the stronger *trans* influence of phosphorus compared with chlorine is again evident. The greater π character of the C═C double bonds compared with the C—C single bonds is again highlighted by their higher ellipticities.

As seen for (1), only 4 of the expected 6 b.c.p.s involving rhodium were identified [Rh—P, Rh—Cl and two Rh—C] during the charge-density analysis. The topological parameters for these interactions again have small positive values for $\rho(r)$ and positive values for $\nabla^2\rho(r)$. Examining the energetics of these interactions it can be seen that they have small negative values for $H(\rho)$ and $|V(\rho)| > G(\rho)$, suggesting some degree of covalency, and a ratio of $|V(\rho)|/G(\rho)$ between 1 and 2 indicating that they again fall into the intermediate region for bonding, see Table 3. The suggestion of an intermediate description of bonding is supported by plots of the Laplacian of $\rho(r)$ around rhodium which shows clear charge concentrations at P1, Cl1 C1 and C4 all directed towards rhodium, indicating some degree of covalency to the interactions, see Fig. 8.

The deformation density maps also show evidence of electron density in the region between Rh and P1/Cl1 combined with a distortion of the electron density in the C1═C2 and C4═C5 bonds, see Fig. 9.

In a similar situation to that seen in (1), the separation between Rh and the C atoms at each end of the norbornadiene cage is very similar, however, only two of the expected b.c.p.s (those to Rh1—C1 and Rh1—C4) were located. Nonetheless, there is evidence of charge concentration at all four C atoms (C1, C2, C4 and C5) directed towards rhodium, suggesting that all four of the C atoms bond to rhodium, see Fig. 8. The Rh—C bond paths are curved (R_{ij} larger than d_{ij}) and the Rh1—C1 and Rh1—C4 b.c.p.s are located in about the region where the r.c.p. might have been expected, see Fig. 10. The [λ_1, λ_2, λ_3]

eigenvalues for Rh1—C1 [−2.08, −0.24, 8.38] and Rh1—C4 [−3.36, −1.36, 12.32] show relatively small values of λ_2, again indicating that the electron density is very flat in one direction perpendicular to the Rh—C bond paths, *i.e.* in the region between rhodium and the two C═C bonds, see Fig. S6. Given these points it seems likely that the two missing b.c.p.s (Rh1—C2, Rh1—C5) result from bond catastrophes having occurred. The evidence strongly suggests that all four C atoms are involved in bonding to the Rh atom, so we shall consider what

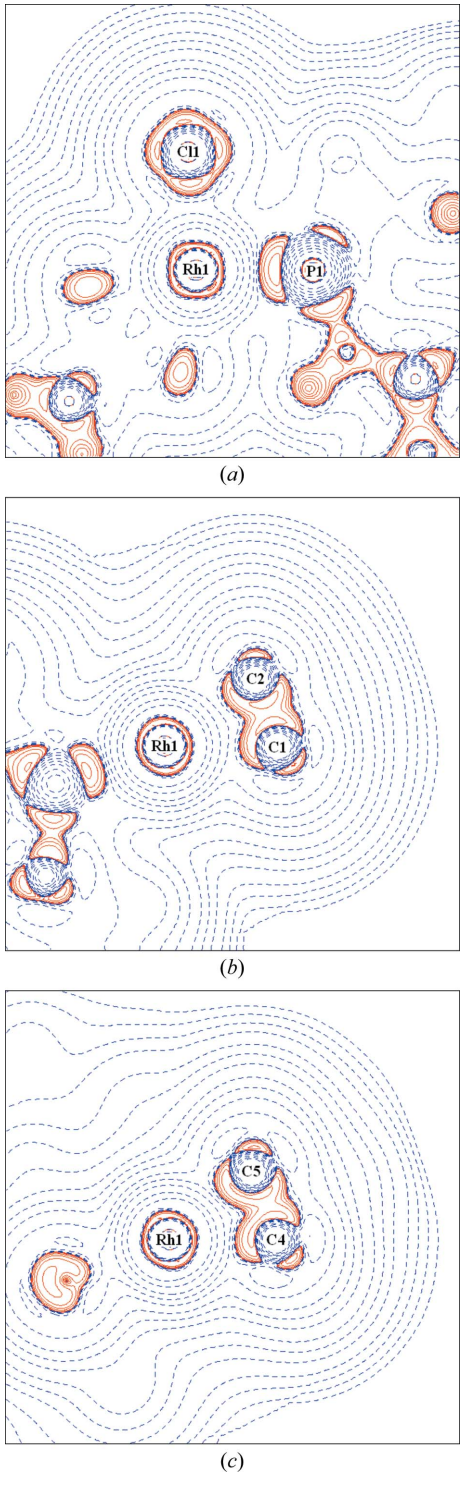

Figure 8
Negative Laplacian of the electron density for [Rh(C_7H_8)(PCy_3)Cl] (2), drawn in the planes (*a*) Rh1—P1—Cl1, (*b*) Rh1—C1—C2 and (*c*) Rh1—C4—C5, with positive contours as solid red lines and negative contours as dashed blue lines.

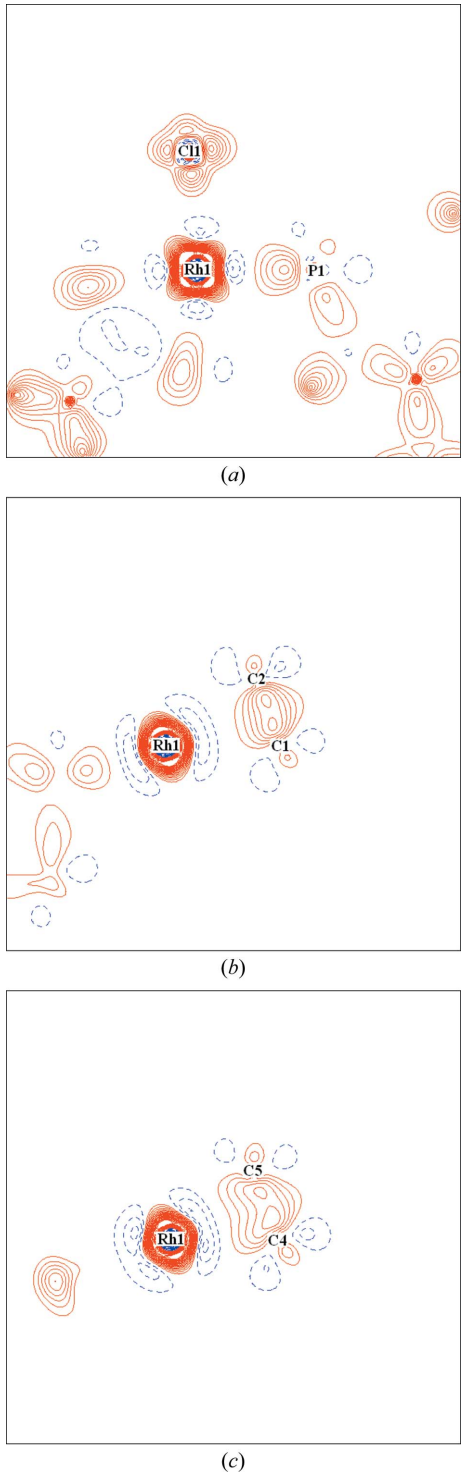

Figure 9
Deformation density map for [Rh(C_7H_8)(PCy_3)Cl] (2), after multipole refinement drawn in (*a*) the Rh1—P1—Cl1 plane, (*b*) Rh1—C1—C2 and (*c*) Rh1—C4—C5. Contours are depicted at the 0.1 e Å^{-3} level, with positive contours as solid red lines and negative contours as dashed blue lines.

Table 4
Topological properties at b.c.p.s involving rhodium in [Rh(C_7H_8)(PPh_3)Cl].

Bond	$\rho(r_{bcp})$ (e Å^{-3})	$\nabla^2\rho(r_{bcp})$ (e Å^{-5})	$H(\rho)$ (a.u.)	$G(\rho)$ (a.u.)	$V(\rho)$ (a.u.)	$\lvert V(\rho)\rvert/G(\rho)$ (a.u.)	ϵ
Rh1—C1	0.57 (1)	5.50 (1)	−0.024	0.085	−0.109	1.282	4.39
Rh1—C4	0.74 (1)	6.73 (1)	−0.046	0.120	−0.166	1.383	2.96
Rh1—C5	0.74 (1)	6.89 (1)	−0.047	0.120	−0.166	1.383	5.28
Rh1—P1	0.68 (1)	3.41 (1)	−0.044	0.085	−0.129	1.518	0.17
Rh1—Cl1	0.57 (1)	6.43 (1)	−0.023	0.091	−0.114	1.253	0.11

can be inferred about the nature of the *M*–alkene interactions. As before, the concave bond paths suggest the presence of sigma donation, with the more pronounced curvature of the Rh1—C1 bond path than the Rh1—C4 bond path suggesting reduced π back-bonding in the former case. Indeed, the Rh1—C1 bond path is 0.078 Å longer than the atom separation compared with 0.018 Å in the case of Rh1—C4. These factors combine to support the assertion that the *trans* influence of phosphorus has weakened the Rh1—C1 bond *trans* to it.

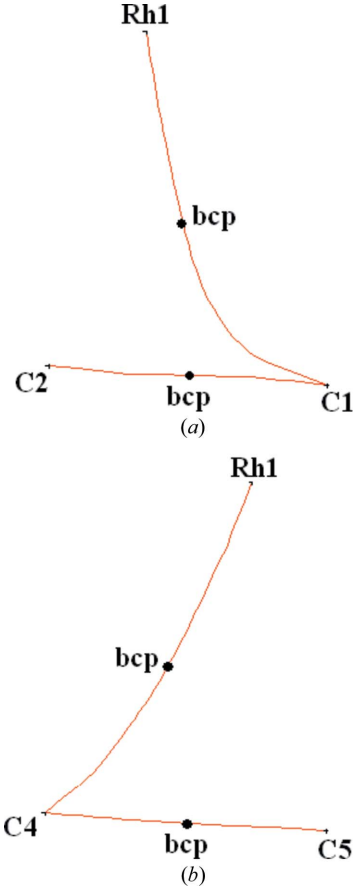

Figure 10
Bond paths in [Rh(C_7H_8)(PCy_3)Cl] (2), between rhodium and the norbornadiene cage with b.c.p.s marked for (*a*) Rh1—C1—C2 and (*b*) Rh—C4—C5.

4. Conclusions

4.1. Comparison between [Rh(C_7H_8)(P^tBu_3)Cl] (1), [Rh(C_7H_8)(PCy_3)Cl] (2) and [Rh(C_7H_8)(PPh_3)Cl] (Sparkes *et al.*, 2008)

Table 4 presents a summary of the topological properties involving rhodium in [Rh(C_7H_8)(PPh_3)Cl] as the values for $H(\rho)$ and $|V(\rho)|/G(\rho)$ were not included in the original paper. As would be expected the three charge-density analyses show very similar results for the topological parameters at b.c.p.s involving rhodium. All of the bonds involving rhodium have positive values of $\rho(r)$ and $\nabla^2\rho(r)$, negative values for $H(\rho)$, $|V(\rho)| > G(\rho)$ and $|V(\rho)|/G(\rho)$ in the range 1–2, suggesting that the bonds fall into the intermediate range of bonding with some degree of covalency, as often seen around heavy atoms.

All three structures have Rh—C b.c.p.s that are missing in regions where they might have been expected. The missing b.c.p.s can be attributed to bond catastrophes having occurred, owing to the flat electron density in the region between Rh and the alkene C=C, which means that only a small change in the electron density can cause b.c.p.s and r.c.p.s to coalesce. Despite this, the presence of charge concentrations at all four C atoms of the norbornadiene in each analysis and distortion to the electron density in the C=C bonds indicates strongly that the four C atoms are, as expected, involved in bonding to rhodium; a fact that would be anticipated on the basis of similar d_{ij} distances between Rh—C for C1 and C2, plus C4 and C5.

The stronger *trans* influence of phosphorus compared with chlorine can be seen in the fact that the Rh—C separations for the C atoms *trans* to phosphorus (C1 and C2) are longer than those for the C atoms *trans* to chlorine (C4 and C5). This is reflected in topological properties of the Rh—C bonds, which have greater electron density, more negative values of $H(\rho)$ and higher values of $|V(\rho)|/G(\rho)$, showing that the bonds are stronger with more covalent character to them. Similarly the C1=C2 bonds are shorter than the C4=C5 bonds by $\sim$ 0.07–0.13 Å and have more π character, as reflected in the higher electron density values at the b.c.p. The concave nature of the bond paths suggests the presence of sigma donation, while the larger curvature of the Rh1 to C1/C2 bond paths compared with those between Rh1 and C4/C5 suggests reduced π back-bonding in the former case.

The authors would like to thank the EPSRC (EP/E048994/1) for funding.

References

Abramov, Yu. A. (1997). *Acta Cryst.* A**53**, 264–272.
Bader, R. F. W. (1990). *Atoms in Molecules: A Quantum Theory*. Oxford University Press.
Bader, R. F. W. & Essén, H. J. (1984). *J. Chem. Phys.* **80**, 1943–1960.
Blessing, R. H. (1997). *J. Appl. Cryst.* **30**, 421–426.

Brayshaw, S. K., Sceats, E. L., Green, J. C. & Weller, A. S. (2007). *Proc. Natl. Acad. Sci. USA*, **104**, 6921–6926.
Chatt, J. & Venanzi, L. M. (1957). *J. Chem. Soc.* pp. 4735–4741.
Clark, R. C. & Reid, J. S. (1995). *Acta Cryst.* A**51**, 887–897.
Cremer, D. & Kraka, E. (1984). *Angew. Chem. Int. Ed.* **23**, 627–628.
Eickerling, G., Mastalerz, R., Herz, V., Scherer, W., Himmel, H.-J. & Reiher, M. (2007). *J. Chem. Theory Comput.* **3**, 2182–2197.
Espinosa, E., Alkorta, I., Elguero, J. & Molins, E. (2002). *J. Chem. Phys.* **117**, 5529–5542.
Farrugia, L. J. (1999). *J. Appl. Cryst.* **32**, 837–838.
Farrugia, L. J., Evans, C. & Tegel, M. (2006). *J. Phys. Chem.* **110**, 7952–7961.
Gatti, C. & Lasi, D. (2007). *Faraday Discuss.* **135**, 55–78.
Gibbs, G. V., Spackman, M. A., Jayatilaka, D., Rosso, K. M. & Cox, D. F. (2006). *J. Phys. Chem. A*, **110**, 12259–12266.
Hansen, N. K. & Coppens, P. (1978). *Acta Cryst.* A**34**, 909–921.
Hirshfeld, F. L. (1976). *Acta Cryst.* A**32**, 239–244.
Jun, C. H. (2004). *Chem. Soc. Rev.* **33**, 610–618.
Macchi, P. & Coppens, P. (2001). *Acta Cryst.* A**57**, 656–662.
Macchi, P., Prosperpio, D. M. & Sironi, A. (1998*a*). *J. Am. Chem. Soc.* **120**, 13429–13435.
Macchi, P., Proserpio, D. M. & Sironi, A. (1998*b*). *J. Am. Chem. Soc.* **120**, 1447–1455.
Overgaard, J., Clausen, H. F., Platts, J. A. & Iversen, B. B. (2008). *J. Am. Chem. Soc.* **130**, 3834–3843.
Overgaard, J., Jones, C., Stasch, A. & Iverson, B. B. (2009). *J. Am. Chem. Soc.* **131**, 4208–4209.
Overgaard, J., Turel, I. & Hibbs, D. E. (2007). *Dalton Trans.* pp. 2171–2178.
Oxford Diffraction (2007). *CrysAlis CCD* and *CrysAlis RED*. Oxford Diffraction Ltd, Abingdon, Oxfordshire, England.
Reisinger, A., Trapp, N., Krossing, I., Altmannshofer, S., Herz, V., Presnitz, M. & Scherer, W. (2007). *Angew. Chem. Int. Ed.* **46**, 8295–8298.
Rybtchinski, B. & Milstein, D. (1999). *Angew. Chem. Int. Ed.* **38**, 870–883.
Scherer, W., Eickerling, G., Shorokhov, D., Gullo, E., McGrady, G. S. & Sirsch, P. (2006). *New J. Chem.* **30**, 309–312.
Sheldrick, G. M. (2008). *Acta Cryst.* A**64**, 112–122.
Sparkes, H. A., Brayshaw, S. K., Weller, A. S. & Howard, J. A. K. (2008). *Acta Cryst.* B**64**, 550–557.
Su, Z. & Coppens, P. (1998). *Acta Cryst.* A**54**, 646–652.
Volkov, A., Macchi, P., Farrugia, L. J., Gatti, C., Mallinson, P., Richter, T. & Koritsanszky, T. (2006). *XD*2006. University at Buffalo, State University of New York, NY, USA; University of Milano, Italy; University of Glasgow, UK; CNRISTM, Milano, Italy; Middle Tennessee State University, TN, USA.